This article has been accepted for publication in a future issue of this journal, but has not been fully edited. Content may change prior to final publication. Citation information: DOI 10.1109/TGRS.2021.3131327, IEEE Transactions on Geoscience and Remote Sensing

Accepted Manuscript
Version of record at: https://doi.org/10.1109/TGRS.2021.3131327

Iterative Implementation Method for Robust Target Localization in a Mixed Interference Environment

Yuan Liu, *Member, IEEE,* Xiang-Gen Xia, *Fellow, IEEE,* Hongwei Liu, *Member, IEEE,* Anh H. T. Nguyen, and Andy W. H. Khong, *Member, IEEE*

***Abstract*—For the problem of target localization under the multipath propagation environment, the existing methods are mainly restricted to the limited prior information of complex reflections, especially when the target is embedded in a mixed interference environment. They may suffer from performance degradation due to the shortage of target classification ability. To address this problem, we propose a target localization method based on iterative implementation with semi-unitary constraint and eigen-decomposition technique, where a practical propagation scenario based on the spherical earth model is considered. Compared to the previous works, the proposed method can automatically distinguish a real target from the mixed interference environment with improved localization accuracy. Neither additional decorrelation preprocessing nor prior information of the dynamic scenario is required. Both simulations and real data experiments validate the effectiveness and robustness of the proposed method.**

***Index Terms*—Complex multipath propagation, direction of arrival (DOA) estimation, mixed interference, semi-unitary constraint, target classification and localization.**

I. Introduction

TARGET localization via direction-of-arrival (DOA) estimation is an essential task in many radar applications, such as radio frequency interference source localization for Earth remote sensing, radar ice sounding, and objects detection and localization [1]–[3]. One of the challenges is the presence of target echo embedded in an unknown multipath propagation environment or in scenarios where interferences are present [4]–[8]. Classical target localization methods may no longer be optimal in such environments resulting in performance deterioration [9], [10]. Solving this problem is non-trivial since the received signals comprise pure target reflection as well as the multiple coherent and uncorrelated interferences, resulting in spatial fluctuation in the received signal's amplitude, phase, and DOA. Moreover, the interfering sources and the target may be too closely spaced with respect to the nominal array resolution.

Over the last few decades, a number of techniques have been developed for target localization [11]–[18]. High-resolution subspace-based methods, such as the multiple signal classification (MUSIC) method [11], combined with the decorrelation preprocessing of spatial smoothing [12] are commonly employed in the presence of multipath propagation. However, the decorrelation process reduces the resolution and the degree of freedom of the radar system. In [13], the relax method based on an iterative search is proposed to address the coherent DOA estimation problem, albeit the extensive multidimensional search of location parameters being required. By exploiting prior information of the multipath propagation environment, a class of refined maximum likelihood (RML) [14], [15] can directly be utilized to achieve efficient target localization performance involving coherent interference with less computation load. The performance of these methods, however, may be limited in practical applications due to model mismatch of the dynamic interference propagation environment.

While the use of accurate prior information can enhance target localization performance in an environment where interfering sources are present, such information may not be readily available [19]. Moreover, prevalent target localization methods are based primarily on the classical two-ray propagation model without considering other reflected waves. Although this model performs reasonably well in a smooth terrain environment, it may lead to a significant model mismatch in a time-varying multipath environment, where an undesired signal (e.g., the spatial distribution of the reflecting paths) may vary with time [20]–[22]. To address this problem, a target localization method was proposed, where the uncertainty of the multipath propagation is considered [21]. However, the performance of this method may be reduced when the low-rank assumption is not satisfied, such as when a target is present in a mixed interference environment. In such a scenario, the ability to classify targets is required to achieve accurate localization performance. This problem has not been addressed in the above-mentioned methods.

We propose a robust target localization algorithm in the presence of interference without the need for additional decorrelation preprocessing or any prior information pertaining to the propagation environment. Our contributions include:

(i) An improved geometric propagation model for target localization is established. This model takes into account the coexistence of both uncorrelated and coherent in-

This work was supported by the National Science Fund for Distinguished Young Scholars under Grant 61525105. (*Corresponding author: Hongwei Liu*)

Yuan Liu is with the School of Electrical and Electronic Engineering, Nanyang Technological University, Singapore 639798, and also with the National Laboratory of Radar Signal Processing, Xidian University, Xi'an 710071, China (e-mail: yuan.liu@ntu.edu.sg).

Xiang-Gen Xia is with the College of Communications, Xidian University, Xi'an 710071, China, and also with the Department of Electrical and Computer Engineering, University of Delaware, Newark, DE 19716 USA (e-mail: xxia@ee.udel.edu).

Hongwei Liu is with the National Laboratory of Radar Signal Processing, Xidian University, Xi'an 710071, China, and also with the Collaborative Innovation Center of Information Sensing and Understanding, Xidian University, Xi'an 710071, China (e-mail: hwliu@xidian.edu.cn).

Anh H. T. Nguyen and Andy W. H. Khong are with the School of Electrical and Electronic Engineering, Nanyang Technological University, Singapore 639798 (e-mail: nguyenhta@ntu.edu.sg; andykhong@ntu.edu.sg).

This article has been accepted for publication in a future issue of this journal, but has not been fully edited. Content may change prior to final publication. Citation information: DOI 10.1109/TGRS.2021.3131327, IEEE Transactions on Geoscience and Remote Sensing

Accepted Manuscript
Version of record at: https://doi.org/10.1109/TGRS.2021.3131327

terferences induced by interfering sources and complex terrain reflections based on the spherical earth model. By taking advantage of the proposed model, the non-practical assumption imposed by the classical two-ray multipath propagation model can be avoided and the effect of the mixed interference can effectively be eliminated. Therefore, the robustness of the propagation model under a practical environment is enhanced.

(ii) A new target localization algorithm based on the iterative implementation of the minimum mean-square error (MMSE) framework with semi-unitary constraint and the eigen-decomposition technique is proposed to ameliorate the influence of interference to achieve accurate estimation of target location parameters. By focusing on the limitation of the prior information in practical applications, DOAs of the incident paths are first detected using the iterative strategy without any prior information about the dynamic environment. The eigen-decomposition technique is subsequently employed to associate the detected reflecting paths with their corresponding target by exploiting the spatial signals' coherence structure. Therefore, a real target can effectively be distinguished from mixed interference environment, resulting in an improved localization performance.

In contrast to the previous works, the proposed method can effectively mitigate the detrimental effects of interference without additional decorrelation preprocessing. The desired target signal can automatically be classified from the mixed interference environment by the proposed method. The main advantages of the proposed method include that it is insensitive to the multipath coherence and it does not require any prior information of the path association and reflections of the illuminated terrain. It also does not require prior knowledge of the sparsity level of spatial interferences. We demonstrate the efficacy of the proposed model and approach via both simulated and experiment results.

The remainder of this paper is organized as follows: Section II establishes the geometric propagation model for target localization in the mixed interference environment. The mathematical model of the received signal is formulated in Section III. Section IV describes the proposed method for target classification and localization in detail. Simulation and experiment results to validate the performance of the proposed method under various scenarios are presented and discussed in Section V. Finally, Section VI concludes the paper.

II. Practical Geometry Model for Target Localization

A target localization scenario is depicted in Fig. 1, where both the complex reflections from the earth's ground surface and the mixed interference are taken into consideration. Points A, B_k, and T denote for the radar site, the kth ground reflection point corresponding to the kth indirect path, and the target position, respectively, where $k = 1, 2, \cdots, K$ with K being the number of the reflecting multipaths from the ground surface. In addition, point markers C, D_k, E, and O represent the projection point of the radar site to the earth

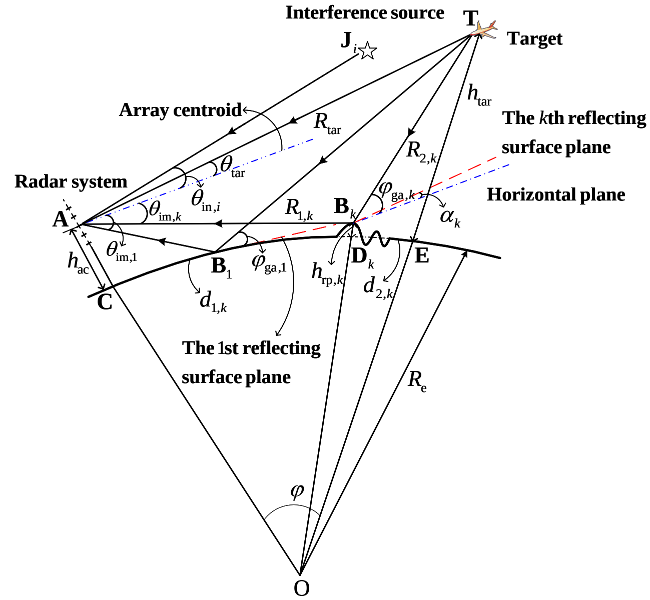

Fig. 1. Propagation geometry model for target localization under the mixed interference environment, where the dashed line, the dash-dotted line, and the double dot dashed line represent the kth reflecting surface plane, the horizontal plane, and the array centroid, respectively.

surface, the kth projection point of B_k to the earth surface, the target's projection point to the earth surface, and the center of the earth, respectively. Path $\mathrm{J}_i\mathrm{A}$ denotes the ith incident interference, where $i = 1, 2, \cdots, I$ with I being the number of the undesired signal paths. Definitions of other parameters involved in Fig. 1 are listed in Table I for convenience.

We aim to derive a set of analytical expressions that establish the relationships among signal propagation in a dynamic environment. These expressions will provide some background for the signal model in Section III and the proposed method in Section IV. The expression of the kth path difference — defined as the difference between the direct path and the kth reflecting path, i.e., $\Delta R_k = R_{1,k} + R_{2,k} - R_{\text{tar}}$ — is first derived. With reference to Fig. 1 and employing the law of cosine to the triangles AOB_k and TOB_k,

$$R_{1,k} = \sqrt{\left(h_{\text{ac}} - h_{\text{rp},k}\right)^2 + 4\left(R_{\text{e}} + h_{\text{ac}}\right)\left(R_{\text{e}} + h_{\text{rp},k}\right)\sin^2\left(\frac{d_{1,k}}{2R_{\text{e}}}\right)} \tag{1}$$

and

$$R_{2,k} = \sqrt{\left(h_{\text{tar}} - h_{\text{rp},k}\right)^2 + 4\left(R_{\text{e}} + h_{\text{tar}}\right)\left(R_{\text{e}} + h_{\text{rp},k}\right)\sin^2\left(\frac{d_{2,k}}{2R_{\text{e}}}\right)}, \tag{2}$$

where R_{e} denotes the equivalent radius of the earth [23]. The variable $R_{\text{e}} = \left(1 + 10^{-6}R_0 dN/dh\right)^{-1} \times R_0$, where $R_0 \approx 6370$ km is the actual radius of the earth [21] and $dN/dh = -39$ N/km is the refractivity gradient [24]. To compute ΔR_k, $d_{1,k}$ in (1) and $d_{2,k}$ in (2) are first determined by computing the length of arc CE and solving

$$\begin{aligned} 2d_{1,k}^3 - 3d_{1,k}^2 d + \left[d^2 - 2\bar{R}_{\text{e},k}\left(\bar{h}_{\text{ac},k} + \bar{h}_{\text{tar},k}\right)\right] \\ \times d_{1,k} + 2\bar{R}_{\text{e},k}\bar{h}_{\text{ac},k} d = 0, \end{aligned} \tag{3}$$

This article has been accepted for publication in a future issue of this journal, but has not been fully edited. Content may change prior to final publication. Citation information: DOI 10.1109/TGRS.2021.3131327, IEEE Transactions on Geoscience and Remote Sensing

Accepted Manuscript
Version of record at: https://doi.org/10.1109/TGRS.2021.3131327

TABLE I
NOMENCLATURE OF THE USED VARIABLES IN FIG. 1

Variables	Definition
θ_{tar}	DOA of the target
$\theta_{\mathrm{im},k}$	DOA of kth reflecting path
$\theta_{\mathrm{in},i}$	DOA of ith interference path
h_{ac}	Array center height
h_{tar}	Target height
$h_{\mathrm{rp},k}$	Height of the kth reflection point
R_{tar}	Target distance
$R_{1,k}$	Distance between radar and kth reflection point
$R_{2,k}$	Distance between target and kth reflection point
$d_{1,k}$	Length of arc CD$_k$
$d_{2,k}$	Length of arc D$_k$E
$\varphi_{\mathrm{ga},k}$	Grazing angle for the kth reflecting surface
α_k	Angle between the horizontal plane and the kth reflecting surface
R_{e}	Equivalent radius of the earth
φ	Angle between CO and EO

for the relationship between $d_{1,k}$ and $d_{2,k}$ [21], [25], where $d = d_{1,k} + d_{2,k}$, $\bar{R}_{\mathrm{e},k} = R_{\mathrm{e}} + h_{\mathrm{rp},k}$, $\bar{h}_{\mathrm{ac},k} = h_{\mathrm{ac}} - h_{\mathrm{rp},k}$, and $\bar{h}_{\mathrm{tar},k} = h_{\mathrm{tar}} - h_{\mathrm{rp},k}$. According to (3), we have

$$d_{1,k} = d_{2,k} - 2\delta_k \sin\left(\frac{\eta_k}{3}\right), \tag{4}$$

where

$$\delta_k = \sqrt{\left(4\bar{R}_{\mathrm{e},k}\left(\bar{h}_{\mathrm{ac},k} + \bar{h}_{\mathrm{tar},k}\right) + d^2\right)/3} \tag{5}$$

and

$$\eta_k = \sin^{-1}\left[-2\bar{R}_{\mathrm{e},k}\left(\bar{h}_{\mathrm{ac},k} - \bar{h}_{\mathrm{tar},k}\right) d/\delta_k^3\right]. \tag{6}$$

By applying the law of cosine to the triangle AOT, we have

$$\begin{aligned} R_{\mathrm{tar}}^2 = {} & \left(R_{\mathrm{e}} + h_{\mathrm{ac}}\right)^2 + \left(R_{\mathrm{e}} + h_{\mathrm{tar}}\right)^2 - 2\left(R_{\mathrm{e}} + h_{\mathrm{ac}}\right) \\ & \times \left(R_{\mathrm{e}} + h_{\mathrm{tar}}\right)\cos\left(\varphi\right), \end{aligned} \tag{7}$$

where $\varphi = d/R_{\mathrm{e}}$. The length of arc CE can then be found using

$$d = 2R_{\mathrm{e}} \sin^{-1}\left(\frac{R_{\mathrm{tar}}^2 - \left(h_{\mathrm{tar}} - h_{\mathrm{ac}}\right)^2}{4\left(R_{\mathrm{e}} + h_{\mathrm{ac}}\right)\left(R_{\mathrm{e}} + h_{\mathrm{tar}}\right)}\right)^{\frac{1}{2}}. \tag{8}$$

We note that the kth path difference ΔR_k can be determined by (1)–(6). It is also worth noting that the attenuation coefficient of the kth reflecting path is dependent on ΔR_k and is required for the simulated scenarios as will be discussed in Section III and Section V, respectively.

With reference to the propagation geometry in Fig. 1, there are two separate paths associated with the target and its kth image, i.e., the direct path (of the target) with incident angle θ_{tar} (measured w.r.t the array centroid) and the kth reflecting path from the ground surface with incident angle $\theta_{\mathrm{im},k}$. The expressions of θ_{tar} and $\theta_{\mathrm{im},k}$ can be derived by applying the law of cosines to the triangle OAT and the law of cosines to the triangle OAB$_k$, respectively, giving

$$\begin{aligned} \left(h_{\mathrm{tar}} + R_{\mathrm{e}}\right)^2 = {} & R_{\mathrm{tar}}^2 + \left(h_{\mathrm{ac}} + R_{\mathrm{e}}\right)^2 - 2R_{\mathrm{tar}} \\ & \times \left(h_{\mathrm{ac}} + R_{\mathrm{e}}\right)\cos\left(\pi/2 + \theta_{\mathrm{tar}}\right), \end{aligned} \tag{9}$$

and

$$\begin{aligned} \left(R_{\mathrm{e}} + h_{\mathrm{rp},k}\right)^2 = {} & R_{1,k}^2 + \left(h_{\mathrm{ac}} + R_{\mathrm{e}}\right)^2 - 2R_{1,k} \\ & \times \left(h_{\mathrm{ac}} + R_{\mathrm{e}}\right)\cos\left(\pi/2 - \theta_{\mathrm{im},k}\right). \end{aligned} \tag{10}$$

The above equations result in

$$\theta_{\mathrm{tar}} = \sin^{-1}\left(\frac{\left(h_{\mathrm{tar}} + R_{\mathrm{e}}\right)^2 - \left(h_{\mathrm{ac}} + R_{\mathrm{e}}\right)^2 - R_{\mathrm{tar}}^2}{2R_{\mathrm{tar}}\left(h_{\mathrm{ac}} + R_{\mathrm{e}}\right)}\right), \tag{11}$$

$$\theta_{\mathrm{im},k} = \sin^{-1}\left(\frac{h_{\mathrm{ac}}^2 + R_{1,k}^2 - h_{\mathrm{rp},k}^2 + 2R_{\mathrm{e}}\left(h_{\mathrm{ac}} - h_{\mathrm{rp},k}\right)}{2\left(h_{\mathrm{ac}} + R_{\mathrm{e}}\right)R_{1,k}}\right). \tag{12}$$

It is worth highlighting that the unknown derived variables θ_{tar} in (11) and $\theta_{\mathrm{im},k}$ in (12) will be required in both the signal model in Section III and the simulated scenarios in Section V. For more information about the effects of complex multipath propagation on target localization accuracy, we refer the reader to the previous works such as presented in [20], [21], and [23].

III. MATHEMATICAL MODEL OF THE RECEIVED SIGNAL

Consider an array radar system comprising M isotropic sensors mounted vertically to the horizontal plane. Assume that there are $I+K+1$ narrowband signals with distinct DOAs impinging on the array. Without loss of generality, suppose the first I signals are uncorrelated interference signals such that the ith path originates from direction $\theta_{\mathrm{in},i}$ corresponding to the propagation of the far field source $s_i(t)$, where $i = 1, 2, \cdots, I$. The remaining $K+1$ coherent signals correspond to the propagation of the far field target $s_{\mathrm{tar}}(t)$, i.e., the direct path signal from direction θ_{tar} and its K multipath reflections impinging on the array from directions $\theta_{\mathrm{im},1}, \cdots, \theta_{\mathrm{im},K}$. In addition, we assume that the target signal and the I interference signals are uncorrelated with each other [26]–[28].

The $M \times 1$ array output at time t can be represented by

$$\begin{aligned} \mathbf{x}(t) &= \left[x_1(t), \cdots, x_m(t), \cdots, x_M(t)\right]^T \\ &= \mu_{\mathrm{tar}}\left(\mathbf{a}\left(\theta_{\mathrm{tar}}\right) + \sum_{k=1}^{K} \rho_k e^{-j2\pi\Delta R_k/\lambda}\mathbf{a}\left(\theta_{\mathrm{im},k}\right)\right) \\ &\quad \times s_{\mathrm{tar}}(t) + \sum_{i=1}^{I}\mathbf{a}\left(\theta_{\mathrm{in},i}\right)s_i(t) + \mathbf{n}(t), \end{aligned} \tag{13}$$

where μ_{tar}, ρ_k, and λ are, respectively, the target scattering coefficient, the specular reflection coefficient of the kth multipath corresponding to the target, and the wavelength, the $M \times 1$ vector $\mathbf{a}(\theta) = \left[1, e^{-j2\pi d_{\mathrm{a}}\sin(\theta)/\lambda}, \cdots, e^{-j2\pi(M-1)d_{\mathrm{a}}\sin(\theta)/\lambda}\right]^T$ is the array steering vector towards direction θ with d_{a} being the inter-element distance, $(\cdot)^T$ is the transpose operator, and $\mathbf{n}(t) = \left[n_1(t), \cdots, n_m(t), \cdots, n_M(t)\right]^T$ given that $n_m(t)$ denotes the additive noise of the mth sensor. We further assume $\mathbf{n}(t)$ is a white Gaussian noise with mean zero and covariance $E\left\{\mathbf{n}(t)\mathbf{n}^H(t)\right\} = \sigma_n^2\mathbf{I}_M$, where $E\{\cdot\}$, $(\cdot)^H$,

Accepted Manuscript
Version of record at: https://doi.org/10.1109/TGRS.2021.3131327

σ_n^2, and $\mathbf{I}_M$ denote the expectation operator, the conjugate transpose, the noise power, and the $M \times M$ identity matrix, respectively.

Equation (13) can further be expressed compactly via

$$\mathbf{x}(t) = \mathbf{B}\mathbf{s}(t) + \mathbf{n}(t), \tag{14}$$

where

$$\mathbf{B} = \left[\mathbf{A}_{\boldsymbol{\theta}_{\text{tar}}}\boldsymbol{\rho}, \mathbf{A}_{\boldsymbol{\theta}_{\text{int}}}\right], \tag{15}$$

$$\mathbf{s}(t) = \left[\mu_{\text{tar}} s_{\text{tar}}(t), \mathbf{s}_{\text{int}}^T(t)\right]^T. \tag{16}$$

Matrices

$$\mathbf{A}_{\boldsymbol{\theta}_{\text{tar}}} = \left[\mathbf{a}(\theta_{\text{tar}}), \mathbf{a}(\theta_{\text{im},1}), \cdots, \mathbf{a}(\theta_{\text{im},k}), \cdots, \mathbf{a}(\theta_{\text{im},K})\right] \tag{17}$$

and

$$\mathbf{A}_{\boldsymbol{\theta}_{\text{int}}} = \left[\mathbf{a}(\theta_{\text{in},1}), \cdots, \mathbf{a}(\theta_{\text{in},i}), \cdots, \mathbf{a}(\theta_{\text{in},I})\right] \tag{18}$$

are formed by the concatenation of the steering vectors given that $\boldsymbol{\theta}_{\text{tar}} = [\theta_{\text{tar}}, \theta_{\text{im},1}, \cdots, \theta_{\text{im},k}, \cdots, \theta_{\text{im},K}]^T$, $\boldsymbol{\theta}_{\text{int}} = [\theta_{\text{in},1}, \cdots, \theta_{\text{in},i}, \cdots, \theta_{\text{in},I}]^T$, and $\boldsymbol{\rho} = [\bar{\rho}_0, \bar{\rho}_1, \cdots, \bar{\rho}_k, \cdots, \bar{\rho}_K]^T$. The variable $\bar{\rho}_k = \rho_k e^{-j2\pi\Delta R_k/\lambda}$ denotes the attenuation coefficient of the kth multipath with $\bar{\rho}_0 = 1$ for the direct-path component. With reference to (13), the $I \times 1$ vector $\mathbf{s}_{\text{int}}(t) = [s_1(t), \cdots, s_i(t), \cdots, s_I(t)]^T$ denotes the signal vector of the interfering sources. We assume that the number of snapshots in a coherent processing interval (CPI) is T_0 and $\boldsymbol{\rho}_{\backslash\bar{\rho}_0} = [\bar{\rho}_1, \cdots, \bar{\rho}_k, \cdots, \bar{\rho}_K]^T$ is not a null vector with the subscript $\backslash\bar{\rho}_0$ denoting the removal of $\bar{\rho}_0$ from $\boldsymbol{\rho}$. Given multichannel observations $\{\mathbf{x}(t)\}_{t=1}^{T_0}$ from an array radar, the key objective is to distinguish the target of interest from the mixed interference environment and achieve accurate target localization by extracting the unknown location parameters. As reported in [20] and [21], it is reasonable to assume that the effect of the target motion can be neglected during the observation time of one CPI since the transmitted waveform of the radar system is narrowband.

To model the propagation channel, we gain insights into the channel parameter ρ_k in (13) since it models the interaction of the kth reflecting path and the correspondingly illuminated area of the ground surface. As described in [29],

$$\rho_k = \rho_{\text{F},k}\rho_{\text{d},k}\rho_{\text{s},k}, \tag{19}$$

where $\rho_{\text{F},k}$, $\rho_{\text{d},k}$, and $\rho_{\text{s},k}$ are the Fresnel reflection coefficient, the divergence factor, and the specular scattering factor for the kth reflecting path, respectively. The Fresnel reflection coefficient $\rho_{\text{F},k}$, is commonly determined by the polarization mode, the grazing angle of the kth reflecting path, and the radar carrier frequency. Expressions for both vertical and horizontal polarizations can be expressed as [30], [31]

$$\rho_{\text{F}_\text{v},k} = \frac{\beta_{\text{cd},k}\sin\varphi_{\text{ga},k} - \sqrt{\beta_{\text{cd},k} - \cos^2\varphi_{\text{ga},k}}}{\beta_{\text{cd},k}\sin\varphi_{\text{ga},k} + \sqrt{\beta_{\text{cd},k} - \cos^2\varphi_{\text{ga},k}}}, \tag{20}$$

and

$$\rho_{\text{F}_\text{h},k} = \frac{\sin\varphi_{\text{ga},k} - \sqrt{\beta_{\text{cd},k} - \cos^2\varphi_{\text{ga},k}}}{\sin\varphi_{\text{ga},k} + \sqrt{\beta_{\text{cd},k} - \cos^2\varphi_{\text{ga},k}}}, \tag{21}$$

where

$$\varphi_{\text{ga},k} = \sin^{-1}\left(\frac{(h_{\text{ac}} + R_\text{e})^2 - R_{1,k}^2 - (h_{\text{tar}} + R_\text{e})^2}{2R_{1,k}(h_{\text{tar}} + R_\text{e})}\right) + \alpha_k \tag{22}$$

denotes the grazing angle of the kth reflecting path obtained by applying the law of cosine to triangle ATB_k. Here, α_k denotes the angle between the horizontal plane and the kth reflecting surface. In (20) and (21), the parameter $\beta_{\text{cd},k}$ — known as the complex dielectric constant — can be achieved by

$$\beta_{\text{cd},k} = \beta_{\text{rd},k} - j\lambda\varepsilon_k/2\pi c\beta_0, \tag{23}$$

where $\beta_{\text{rd},k}$, ε_k, and c are, respectively, the relative dielectric constant, the conductivity of the kth reflecting surface, and the speed of light with $\beta_0 = 8.85 \times 10^{-12}$ F/m.

Without loss of generality, the second factor $\rho_{\text{d},k}$ is introduced since the power of the multipath reflected by a spherical reflecting surface is expected to be lower than that reflected by a flat reflecting surface. Considering the curvature of the earth surface [25]

$$\rho_{\text{d},k} \approx \left(\sqrt{1 + \frac{2d_{1,k}d_{2,k}}{R_\text{e}(d_{1,k} + d_{2,k})\sin\alpha_k}}\right)^{-1}. \tag{24}$$

The last factor $\rho_{\text{s},k}$, models the reduction effect of the reflecting path caused by the rugged topography of the practical terrain [32], [33] and is given by

$$\rho_{\text{s},k} = \begin{cases} e^{-8\pi^2\gamma_k^2}, & 0 \le \gamma_k \le 0.1; \\ \frac{0.8125}{1+8(\pi\gamma_k)^2}, & \gamma_k > 0.1. \end{cases} \tag{25}$$

Here, $\gamma_k = \sigma_{\text{sd}}\sin\varphi_{\text{ga},k}/\lambda$ is the roughness factor with σ_{sd} denoting the standard deviation of the terrain height distribution.

IV. Proposed Method for Target Localization

We propose a target localization method based on the iterative implementation of the MMSE framework with semi-unitary constraint and eigen-decomposition technique. The proposed method can cope with the challenging interference environment and is implemented in the following three steps. Firstly, the respective DOAs of the incident paths are detected and estimated using an iterative strategy. The detected paths are subsequently associated with different groups by employing eigen-decomposition with a combinatorial optimization method. Finally, accurate target location is achieved by exploiting the path association information and the geometrical relationship of the target tracking scenario.

A. DOA Estimation Based on Iterative Implementation

DOAs of individual paths are estimated based on an iterative structured implementation of the MMSE framework without any prior knowledge of the spatial sources. By exploiting the signal's sparseness characteristic in the spatial domain, we formulate the received signal model in (14) as a parameterized version. An overcomplete dictionary of size $M \times N$ is firstly constructed as

$$\mathbf{D} = \left[\mathbf{a}(\theta_1), \mathbf{a}(\theta_2), \cdots, \mathbf{a}(\theta_n), \cdots, \mathbf{a}(\theta_N)\right], \tag{26}$$

Accepted Manuscript
Version of record at: https://doi.org/10.1109/TGRS.2021.3131327

where $n = 1, \cdots, N$ with N being the number of potential path directions and $\{\theta_n\}_{n=1}^{N}$ is the sampling grid set of the potential directions of interesting paths with $N \gg M$. Using an overcomplete representation, the problem in (14) can then be reformulated as

$$\mathbf{x}(t) = \mathbf{D}\boldsymbol{\xi}(t) + \mathbf{n}(t), \tag{27}$$

where $\boldsymbol{\xi}(t) \in \mathbb{C}^{N\times 1}$ denotes the sparse (parameterized) coefficient vector with the nth element

$$\xi_n(t) = \begin{cases} \mu_{\mathrm{tar}} s_{\mathrm{tar}}(t), & \theta_n = \theta_{\mathrm{tar}}; \\ \bar{\rho}_k s_{\mathrm{tar}}(t), & \theta_n = \theta_{\mathrm{im},k}, k = 1, 2, \cdots, K; \\ s_i(t), & \theta_n = \theta_{\mathrm{in},i}, \ \ i = 1, 2, \cdots, I; \\ 0, & \text{otherwise.} \end{cases} \tag{28}$$

With sufficient quantization of the sampling grid, we infer from (14) and (27) that $\boldsymbol{\xi}(t)$ will, in theory, consist of all zeros except for $I + K + 1$ non-zero elements corresponding to the paths of the target and the interference sources. The overcomplete representation in (27) makes it possible to reformulate the DOA estimation problem as estimating $\boldsymbol{\xi}(t)$, from which the DOAs of the incident paths can be determined [34].

Based on the observed data $\mathbf{x}(t)$ in (27), the objective of the proposed DOA estimation technique is to estimate the $M \times N$ adaptive filter bank $\mathbf{W}$ and $\boldsymbol{\xi}$ via the cost function

$$\left(\widehat{\boldsymbol{\xi}}, \widehat{\mathbf{W}}\right) = \arg\min_{\boldsymbol{\xi},\mathbf{W}} f(\boldsymbol{\xi}, \mathbf{W}), \quad \text{s.t.} \mathbf{W}\mathbf{W}^H = \mathbf{I}_M, \tag{29}$$

where $f(\boldsymbol{\xi}, \mathbf{W}) = \left\|\boldsymbol{\xi} - \mathbf{W}^H\mathbf{x}\right\|_2^2$ with $\|\cdot\|_2$ being the ℓ_2-norm, $\mathbf{I}_M$ denotes the $M \times M$ identity matrix, and the semi-unitary constraint is employed to avoid dual zero solutions. For brevity, we have removed the time indices in (29) and the remainder of this paper.

To solve (29), we introduce an iterative optimization strategy [35]–[37] implemented by alternating between updating the estimate of $\mathbf{W}$ and the estimate of $\boldsymbol{\xi}$. The optimization strategy starts with the initial estimate of $\boldsymbol{\xi}$ by employing the matched filter bank [38] such that

$$\widehat{\boldsymbol{\xi}}_0 = \mathbf{D}^H\mathbf{x}. \tag{30}$$

Defining $\widehat{\boldsymbol{\xi}}_q$ and $\widehat{\mathbf{W}}_q$ as the estimated parameterized vector and adaptive filter bank in the qth iteration, respectively, the method estimates $\widehat{\mathbf{W}}_{q+1}$ by minimizing the cost function $f(\boldsymbol{\xi}, \mathbf{W})$ in (29) via

$$\widehat{\mathbf{W}}_{q+1} = \arg\min_{\mathbf{W}} \left\|\widehat{\boldsymbol{\xi}}_q - \mathbf{W}^H\mathbf{x}\right\|_2^2, \quad \text{s.t.} \mathbf{W}\mathbf{W}^H = \mathbf{I}_M. \tag{31}$$

It is important to note that the above optimization is not convex. A re-parameterization method was proposed in [39] to simplify the above optimization of the unitary constrained problem. Instead of finding a general unitary matrix that minimizes the cost function in (31), a full-row rank matrix $\mathbf{F}$ was proposed to minimize the cost function, i.e.,

$$\mathbf{F}_{q+1} = \arg\min_{\mathbf{F}} \left\|\widehat{\boldsymbol{\xi}}_q - \mathbf{W}^H\mathbf{x}\right\|_2^2, \quad \text{s.t.} \mathbf{W} = \left(\mathbf{F}\mathbf{F}^H\right)^{-\frac{1}{2}}\mathbf{F}. \tag{32}$$

Algorithm 1 Accelerated optimization scheme

Input: Received data collection $\mathbf{x}$, overcomplete dictionary $\mathbf{D}$, step size η and threshold $\Delta\mu_1$;

$\mu \leftarrow 1$, $\mathbf{F}_0 \leftarrow \mathbf{D}$, $\mathbf{H}_0 \leftarrow \mathbf{F}_0$, $G_0^{\mathrm{in}} \leftarrow 0$;
for $g = 0, 1, \cdots, G$ **do**
  Compute $\nabla_{\mathbf{H}^*} f\left(\widehat{\boldsymbol{\xi}}_q, \left(\mathbf{H}_q\mathbf{H}_q^H\right)^{-\frac{1}{2}}\mathbf{H}_q\right)$ by (33);
  $\mathbf{F}_{g+1} \leftarrow \mathbf{H}_q - \eta\nabla_{\mathbf{H}^*} f\left(\widehat{\boldsymbol{\xi}}_q, \left(\mathbf{H}_q\mathbf{H}_q^H\right)^{-\frac{1}{2}}\mathbf{H}_q\right)$;
  $\mathbf{H}_{g+1} \leftarrow \mathbf{F}_{g+1} + (\mu - 1)/(\mu + 2)\left(\mathbf{F}_{g+1} - \mathbf{F}_g\right)$;
  $G_{g+1}^{\mathrm{in}} \leftarrow \left\|\widehat{\boldsymbol{\xi}}_q - \left(\left(\mathbf{F}_{g+1}\mathbf{F}_{g+1}^H\right)^{-\frac{1}{2}}\mathbf{F}_{g+1}\right)^H\mathbf{x}\right\|_2^2$;
  if $\left|G_{g+1}^{\mathrm{in}} - G_g^{\mathrm{in}}\right| \leq \Delta\mu_1$ **then**
    Break the iteration
  else
    $\mu \leftarrow \mu + 1$;
  end if
end for
$\widehat{\mathbf{W}}_{q+1} \leftarrow \left(\widehat{\mathbf{F}}_{\mathrm{opt}}\widehat{\mathbf{F}}_{\mathrm{opt}}^H\right)^{-\frac{1}{2}}\widehat{\mathbf{F}}_{\mathrm{opt}}$,where $\widehat{\mathbf{F}}_{\mathrm{opt}}$ is the final estimation of $\mathbf{F}$;

Output: Estimation of $\widehat{\mathbf{W}}_{q+1}$.

According to the Lemma 1 stated in [39], the Euclidean gradient of the cost function $f\left(\widehat{\boldsymbol{\xi}}_q, \left(\mathbf{F}\mathbf{F}^H\right)^{-\frac{1}{2}}\mathbf{F}\right)$ w.r.t. $\mathbf{F}^*$ can be computed using

$$\nabla_{\mathbf{F}^*} f\left(\widehat{\boldsymbol{\xi}}_q, \left(\mathbf{F}\mathbf{F}^H\right)^{-\frac{1}{2}}\mathbf{F}\right) = \mathbf{U}\left(\mathbf{C}^H + \mathbf{C}\right)\boldsymbol{\Sigma}\mathbf{V}^H + \mathbf{U}\boldsymbol{\Sigma}^{-1} \times \mathbf{U}^H\nabla_{\mathbf{W}^*} f\left(\widehat{\boldsymbol{\xi}}_q, \mathbf{W}\right). \tag{33}$$

In (33), the matrix $\mathbf{F} = \mathbf{U}\boldsymbol{\Sigma}\mathbf{V}^H$ is decomposed using economy-sized singular value decomposition (eSVD), where $\mathbf{U} \in \mathbb{C}^{M\times M}$ is a unitary matrix whose columns are the left-singular vectors of $\mathbf{F}$, $\boldsymbol{\Sigma} \in (0, \infty)^{M\times M}$ is a diagonal matrix with entries being the singular values of $\mathbf{F}$, $\mathbf{V} \in \mathbb{C}^{N\times M}$ is a semi-unitary matrix with columns being the right-singular vectors of $\mathbf{F}$, $\nabla_{\mathbf{W}^*} f\left(\widehat{\boldsymbol{\xi}}_q, \mathbf{W}\right)$ denotes the gradient of $f\left(\widehat{\boldsymbol{\xi}}_q, \mathbf{W}\right)$ w.r.t. $\mathbf{W}^*$ with $(\cdot)^*$ being the conjugation operator, and $\mathbf{W} = \left(\mathbf{F}\mathbf{F}^H\right)^{-\frac{1}{2}}\mathbf{F} = \mathbf{U}\mathbf{V}^H$. In addition,

$$\mathbf{C} = -\left(\boldsymbol{\Sigma}^{-1}\mathbf{U}^H\nabla_{\mathbf{W}^*} f\left(\widehat{\boldsymbol{\xi}}_q, \mathbf{W}\right)\mathbf{V}\right) \oslash \left(\mathbf{1}_M\boldsymbol{\sigma}^T + \boldsymbol{\sigma}\mathbf{1}_M^T\right), \tag{34}$$

where $\boldsymbol{\sigma}^T$, $\mathbf{1}_M$, and $\oslash$ are the diagonal vector of $\boldsymbol{\Sigma}$, the all-one column vector, and the element-wise division operator, respectively.

With reference to (33), existing optimization algorithms such as the Nesterov accelerated gradient algorithm [40], can be employed to solve (32) to obtain the $(q + 1)$th estimate $\widehat{\mathbf{W}}_{q+1}$. Algorithm 1 summarizes the above approach.

To update the estimate of $\boldsymbol{\xi}$ in the $(q + 1)$th iteration, we then minimize $f(\boldsymbol{\xi}, \mathbf{W})$ w.r.t. $\boldsymbol{\xi}_{q+1}$ resulting in

$$\widehat{\boldsymbol{\xi}}_{q+1} = \widehat{\mathbf{W}}_{q+1}^H\mathbf{x}. \tag{35}$$

The above process is repeated until a stop criterion is satisfied and the final estimate $\widehat{\boldsymbol{\xi}}_{\mathrm{opt}} \in \mathbb{C}^{N\times 1}$ can then be obtained. Elements within $\widehat{\boldsymbol{\xi}}_{\mathrm{opt}}$, therefore, describe the estimated spatial

Accepted Manuscript
Version of record at: https://doi.org/10.1109/TGRS.2021.3131327

spectrum corresponding to the spatial signals impinging on the array. Defining $\mathbb{N}$ as the set of indices n corresponding to peaks of the following function

$$P_{\text{Spec}}\left(n\right)=10\log_{10}\left(\left|\widehat{\boldsymbol{\xi}}_{\text{opt}}\left(n\right)\right|^{2}\right), \tag{36}$$

where $\widehat{\boldsymbol{\xi}}_{\text{opt}}\left(n\right)$ denotes the nth element of $\widehat{\boldsymbol{\xi}}_{\text{opt}}$, the set of estimated DOA is then given by

$$\widehat{\boldsymbol{\theta}}=\left\{\theta_{n}\mid n\in\mathbb{N}\right\}. \tag{37}$$

B. Target Classification via Eigen-decomposition Technique

To identify and locate a target accurately in the complex interference environment, it is necessary to discriminate paths associated with the target and the interference sources via the process of path association [41]. We employ the subspace method [1]–[3], [10], [11] for target classification. According to $\mathbf{x}\left(t\right)$ in (14), the array covariance matrix can be expressed as

$$\begin{aligned}\mathbf{R}_{\text{x}}=&E\left\{\mathbf{x}\left(t\right)\mathbf{x}^{H}\left(t\right)\right\}\\=&\mathbf{B}\mathbf{R}_{s}\mathbf{B}^{H}+\sigma_{n}^{2}\mathbf{I}_{M},\end{aligned} \tag{38}$$

where the signal covariance matrix $\mathbf{R}_{s}=E\left\{\mathbf{s}\left(t\right)\mathbf{s}^{H}\left(t\right)\right\}\in\mathbb{C}^{(I+1)\times(I+1)}$ is positive definite since the target signal and all the interference signals are statistically independent each other.

We claim that when $M\geq I+K+1$, matrix $\mathbf{B}$ is of full column rank and rank $\left(\mathbf{B}\mathbf{R}_{s}\mathbf{B}^{H}\right)=I+1$. The proof is given in Appendix A. Therefore, matrix $\mathbf{R}_{\text{x}}$ has only I+1 large eigenvalues as opposed to $I+K+1$ number of all incident paths. Performing eigenvalue decomposition (EVD) on $\mathbf{R}_{\text{x}}\in\mathbb{C}^{M\times M}$ results in

$$\mathbf{R}_{\text{x}}=\mathbf{U}_{s}\boldsymbol{\Lambda}_{s}\mathbf{U}_{s}^{H}+\mathbf{U}_{n}\boldsymbol{\Lambda}_{n}\mathbf{U}_{n}^{H}, \tag{39}$$

where $\boldsymbol{\Lambda}_{s}\in\left(0,\infty\right)^{(I+1)\times(I+1)}$ and $\boldsymbol{\Lambda}_{n}\in\left(0,\infty\right)^{(M-I-1)\times(M-I-1)}$ are two diagonal matrices with diagonal elements representing, respectively, the eigenvalues of the signal and the noise, $\mathbf{U}_{s}\in\mathbb{C}^{M\times(I+1)}$ denotes eigenvectors corresponding to the I+1 larger eigenvalues, and $\mathbf{U}_{n}\in\mathbb{C}^{M\times(M-I-1)}$ denotes eigenvectors associated with the remaining small eigenvalues. Matrices $\mathbf{U}_{s}$ and $\mathbf{U}_{n}$ span the signal- and noise-subspace, respectively, and since these subspaces are orthogonal to each other, we have

$$\text{span}\left(\mathbf{B}\right)=\text{span}\left(\mathbf{U}_{s}\right)=\text{null}\left(\mathbf{U}_{n}^{H}\right), \tag{40}$$

where span $\left(\mathbf{B}\right)$, span $\left(\mathbf{U}_{s}\right)$, and null $\left(\mathbf{U}_{n}^{H}\right)$ are the range space of $\mathbf{B}$, the range space of $\mathbf{U}_{s}$, and the null space of $\mathbf{U}_{n}^{H}$, respectively. It is important to note that the signal subspace is spanned by the columns of $\mathbf{B}$ and exploiting the property in (40), we have

$$\left\|\mathbf{U}_{n}^{H}\mathbf{B}\right\|_{F}=\left\|\mathbf{U}_{n}^{H}\left[\mathbf{A}_{\boldsymbol{\theta}_{\text{tar}}}\boldsymbol{\rho},\mathbf{A}_{\boldsymbol{\theta}_{\text{int}}}\right]\right\|_{F}=0, \tag{41}$$

where $\left\|\cdot\right\|_{F}$ stands for the Frobenius norm. Therefore,

$$\left\|\left(\mathbf{A}_{\boldsymbol{\theta}_{\text{tar}}}\boldsymbol{\rho}\right)^{H}\mathbf{U}_{n}\right\|_{2}=\left\|\bar{\mathbf{a}}^{H}\left(\boldsymbol{\theta}_{\text{tar}},\boldsymbol{\rho}\right)\mathbf{U}_{n}\right\|_{2}=0, \tag{42}$$

and

$$\left\|\mathbf{a}^{H}\left(\theta_{\text{in},i}\right)\mathbf{U}_{n}\right\|_{2}=0,\quad i=1,2,\cdots,I, \tag{43}$$

where $\bar{\mathbf{a}}\left(\boldsymbol{\theta}_{\text{tar}},\boldsymbol{\rho}\right)=\mathbf{a}\left(\theta_{\text{tar}}\right)+\sum_{k=1}^{K}\bar{\rho}_{k}\mathbf{a}\left(\theta_{\text{im},k}\right)$ is the linear combination of the steering vectors corresponding to the target.

From (40), (42), and (43), we have $\bar{\mathbf{a}}\left(\boldsymbol{\theta}_{\text{tar}},\boldsymbol{\rho}\right)\in\text{span}\left(\mathbf{U}_{s}\right)$, $\mathbf{a}\left(\theta_{\text{in},i}\right)\in\text{span}\left(\mathbf{U}_{s}\right)$, and the signal subspace is spanned by the steering vectors of the interfering sources and the linear combination of the steering vectors of the target paths. However, for subspace-based DOA estimation methods (e.g., as the classical MUSIC method), it is known that the signal subspace may diffuse into the noise subspace in a multipath propagation environment due to the highly correlated nature of the target signals. In fact, we have the following result.

With the above formulations, we claim that $\mathbf{a}\left(\theta_{\text{tar}}\right)\notin\text{span}\left(\mathbf{U}_{s}\right)$ and $\mathbf{a}\left(\theta_{\text{im},k}\right)\notin\text{span}\left(\mathbf{U}_{s}\right)$. The proof is given in Appendix B. Therefore, we have

$$\left\|\mathbf{a}^{H}\left(\theta_{\text{tar}}\right)\mathbf{U}_{n}\right\|_{2}\neq0, \tag{44}$$

and

$$\left\|\mathbf{a}^{H}\left(\theta_{\text{im},k}\right)\mathbf{U}_{n}\right\|_{2}\neq0,\quad k=1,2,\cdots,K. \tag{45}$$

According to (43)–(45), the MUSIC pseudospectrum [1]–[3], [10], [11]

$$g\left(\theta,\mathbf{U}_{n}\right)=\frac{1}{\mathbf{a}^{H}\left(\theta\right)\mathbf{U}_{n}\mathbf{U}_{n}^{H}\mathbf{a}\left(\theta\right)} \tag{46}$$

generates a peak for any direction θ corresponding to the I interference paths, i.e., if $\theta\in\left\{\theta_{\text{in},1},\cdots,\theta_{\text{in},I}\right\}\triangleq\widehat{\boldsymbol{\theta}}_{\text{int}}$, while peaks do not exist for any direction θ corresponding to the target paths, i.e., if $\theta\in\left\{\theta_{\text{tar}},\theta_{\text{im},1},\cdots,\theta_{\text{im},K}\right\}\triangleq\widehat{\boldsymbol{\theta}}_{\text{tar}}$. This is also the reason why the classical MUSIC method described by (46) does not achieve good performance in a multipath propagation environment. Under such operating condition, decorrelation preprocessing is required to mitigate the detrimental effect of multipath on target localization accuracy described in Section I.

In addition, $\forall i\in\left\{1,2,\cdots,I\right\}$ and $\forall k\in\left\{1,2,\cdots,K\right\}$, we have

$$g\left(\theta_{\text{in},i},\mathbf{U}_{n}\right)>g\left(\theta_{\text{tar}},\mathbf{U}_{n}\right), \tag{47}$$

and

$$g\left(\theta_{\text{in},i},\mathbf{U}_{n}\right)>g\left(\theta_{\text{im},k},\mathbf{U}_{n}\right). \tag{48}$$

The above analysis can be used to address the target classification problem without any prior knowledge of the attenuation coefficients $\left\{\bar{\rho}_{k}\right\}_{k=1}^{K}$ that are generally unknown in practical applications.

Since the target signal and all the interference signals are statistically independent of each other, conventional estimation algorithms such as MDL and AIC [42]–[44], can be employed to identify I number of interfering sources. Therefore, we assume I is known apriori. According to the properties of (47) and (48), the DOA association set of interfering sources $\widehat{\boldsymbol{\theta}}_{\text{int}}$ can be identified by selecting elements that generate I largest values of the objective function $g\left(\theta,\mathbf{U}_{n}\right)$ from $\widehat{\boldsymbol{\theta}}$ in (37). The association set of the target paths can accordingly be determined via the set difference of $\widehat{\boldsymbol{\theta}}$ and $\widehat{\boldsymbol{\theta}}_{\text{int}}$, i.e., $\widehat{\boldsymbol{\theta}}_{\text{tar}}=\widehat{\boldsymbol{\theta}}\setminus\widehat{\boldsymbol{\theta}}_{\text{int}}$ with $\setminus$ denoting the set subtraction. Therefore, the final estimate of the target direction denoted by $\widehat{\theta}_{\text{tar}}$ can

Accepted Manuscript
Version of record at: https://doi.org/10.1109/TGRS.2021.3131327

Algorithm 2 Proposed target classification and localization algorithm

Input: Received data collection $\mathbf{x}$, overcomplete dictionary $\mathbf{D}$, the maximum iteration number Q and threshold $\Delta\mu_2$;
1: $q \leftarrow 0$, $G_0^{\text{out}} \leftarrow 0$;
2: Compute the initial parameterized vector $\widehat{\boldsymbol{\xi}}_q$ by (30);
3: **while** $q \leq Q$ **do**
4: Update $\widehat{\mathbf{W}}_{q+1}$ by using Algorithm 1 in Section IV-A;
5: Update $\widehat{\boldsymbol{\xi}}_{q+1}$ by (35);
6: Compute $G_{q+1}^{\text{out}} = \left\| \widehat{\boldsymbol{\xi}}_{q+1} - \mathbf{W}_{q+1}^H \mathbf{x} \right\|_2^2$;
7: **if** $\left| G_{q+1}^{\text{out}} - G_q^{\text{out}} \right| \leq \Delta\mu_2$ **then**
8: Break the iteration
9: **else**
10: $q \leftarrow q + 1$. Go to step 4;
11: **end if**
12: **end while**
13: Identify $\widehat{\boldsymbol{\theta}}$ by implementing the peak-searching operation to $P_{\text{Spec}}(n)$ in (36);
14: Achieve the noise subspace $\mathbf{U}_n$ by (39);
15: Identify $\widehat{\boldsymbol{\theta}}_{\text{int}}$ by selecting the elements that generate I largest values of the objective function $g(\theta, \mathbf{U}_n)$ from $\widehat{\boldsymbol{\theta}}$ in (37);
16: Identify the estimation of the real target direction $\widehat{\theta}_{\text{tar}}$ from $\widehat{\boldsymbol{\theta}}_{\text{tar}} = \widehat{\boldsymbol{\theta}} \backslash \widehat{\boldsymbol{\theta}}_{\text{int}}$ by exploiting the spatial relationship between the direct and reflecting paths with respect to the horizontal plane;
17: Compute the target height $\widehat{h}_{\text{tar}}$ by (49).

Output: Estimation of target height $\widehat{h}_{\text{tar}}$.

be identified from $\widehat{\boldsymbol{\theta}}_{\text{tar}}$, where directions of the direct and reflecting paths of the target are, in general, separated by the horizontal plane based on the geometric relationship of the multipath propagation as reported in [20]–[22]. It is worth mentioning that the focus of this paper is addressing the target localization problem under multipath propagation environment with uncorrelated interferences. We therefore expect that the performance may be reduced for correlated interferers. By considering this, we refer some exist algorithms that focus on correlated interferers [45]–[47].

C. Target Height Computation Based on Spherical Earth Model

With reference to the geometrical relationship of the propagation model described in Section II, the target height can be estimated via the law of cosine to the triangle AOT with $\widehat{\theta}_{\text{tar}}$ giving

$$\widehat{h}_{\text{tar}} = \sqrt{R_{\text{tar}}^2 + (h_{\text{ac}} + R_{\text{e}})^2 + 2R_{\text{tar}}(h_{\text{ac}} + R_{\text{e}}) \sin\left(\widehat{\theta}_{\text{tar}}\right)} - R_{\text{e}}. \tag{49}$$

For clarity, the complete procedure of the proposed target classification and localization method is summarized in Algorithm 2.

TABLE II
SIMULATION SETUP FOR THE FIRST SIMULATION

Parameters	Value or mode
Polarization pattern	Horizontal polarization
Height of the array center	80 m
Number of snapshots	64
Interference source direction	$-10°$ and $10°$
Reflection point height	5 m
Relative dielectric constant	7
Number of iterations	10
Conductivity	4×10^{-2} S/m
Standard deviation	0.15 m
Target distance	80 km
Target height	5 km and 8.5 km
Halt threshold	10^{-5}

V. RESULTS

A. Simulation Results

We conduct simulations to evaluate the performance of the proposed method, where a 22-sensor uniform linear array (ULA) with half-wavelength element spacing is employed. Estimation performance associated with target direction and height are evaluated in terms of root-mean-square error (RMSE)

$$\text{RMSE}_{\theta_{\text{tar}}} = \sqrt{\frac{1}{L_{\text{Mon}}} \sum_{l=1}^{L_{\text{Mon}}} \left(\widehat{\theta}_{\text{tar},l} - \theta_{\text{tar}}\right)^2} \tag{50}$$

and

$$\text{RMSE}_{h_{\text{tar}}} = \sqrt{\frac{1}{L_{\text{Mon}}} \sum_{l=1}^{L_{\text{Mon}}} \left(\widehat{h}_{\text{tar},l} - h_{\text{tar}}\right)^2}, \tag{51}$$

where $\widehat{\theta}_{\text{tar},l}$ and $\widehat{h}_{\text{tar},l}$ are, respectively, the estimates of θ_{tar} and h_{tar} in the lth trial, and L_{Mon} is the number of Monte Carlo trials. We compare the performance of our proposed method to baseline algorithms including SS-MUSIC [12], the relax method [13], the RML method [15], and that described in [21] under various scenarios. Similar to the simulations performed in [6] and [8], we assume that the interference sources and the target have the same power. In particular, to reflect actual deployment, information pertaining to path association is not provided to the proposed method. In contrast, the baseline algorithms require such information to achieve reasonable performance.

In the first simulation, we investigate the performance of DOA and elevation estimation involving a horizontal reflecting surface and well-separated interferers. In this simulation, the information pertaining to the multipath propagation is unknown and the other parameters for the simulation setup are listed in Table II. How the RMSE varies with signal-to-noise ratio (SNR) is shown in Fig. 2, where the target is located at 80 km from the radar with a height of 5 km for Fig. 2(a)–(b) and 8.5 km for Fig. 2(c)–(d). We note that the performance of the RML method is severely impacted even under high

This article has been accepted for publication in a future issue of this journal, but has not been fully edited. Content may change prior to final publication. Citation information: DOI 10.1109/TGRS.2021.3131327, IEEE Transactions on Geoscience and Remote Sensing

Accepted Manuscript
Version of record at: https://doi.org/10.1109/TGRS.2021.3131327

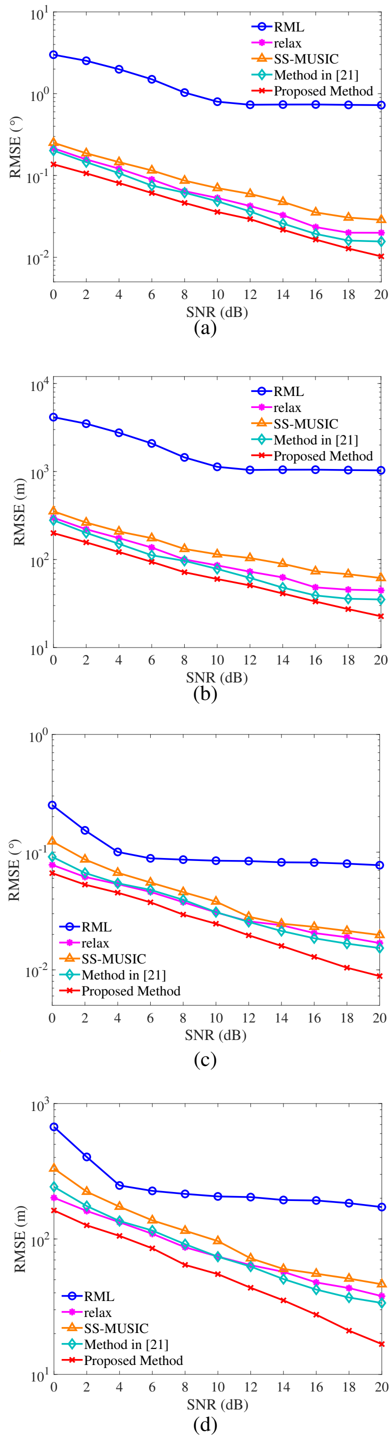

Fig. 2. Variation of RMSE in terms of DOA and height estimates with input SNR in the scenario involving a horizontal reflecting surface and well-separated interferences. (a) Target direction estimation for h_{tar} = 5 km. (b) Target height estimation for h_{tar} = 5 km. (c) Target direction estimation for h_{tar} = 8.5 km. (d) Target height estimation for h_{tar} = 8.5 km. All results at every given SNR are averaged over 500 Monte Carlo trials.

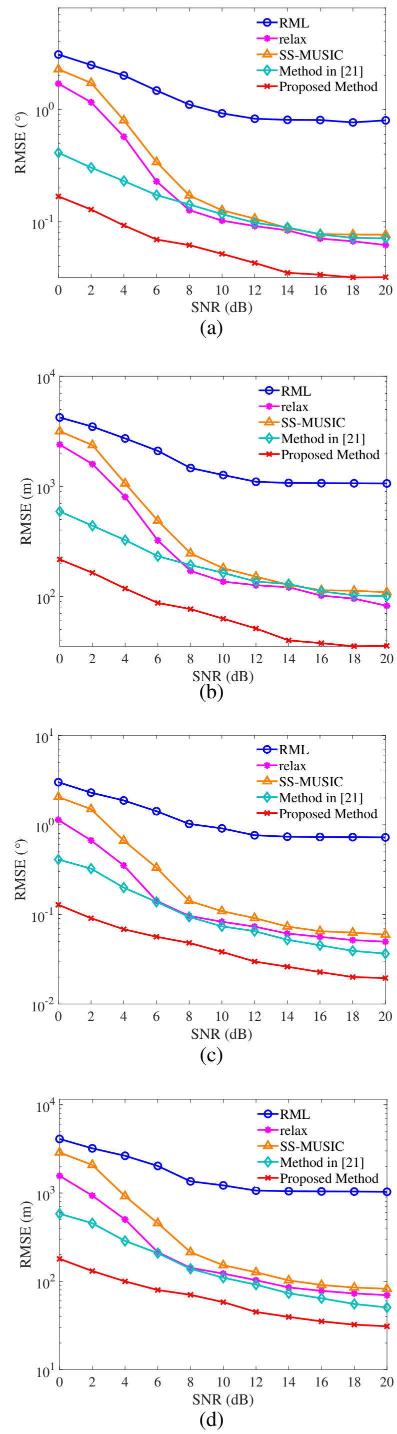

Fig. 3. Variation of RMSE in terms of DOA and height estimates with input SNR in the scenario involving two reflecting surfaces and closely spaced interferences. (a) Target direction estimation for h_{tar} = 6 km. (b) Target height estimation for h_{tar} = 6 km. (c) Target direction estimation for h_{tar} = 9 km. (d) Target height estimation for h_{tar} = 9 km. All results at every given SNR are averaged over 500 Monte Carlo trials.

SNR conditions. This is due to the model mismatch of the conventional symmetric multipath propagation model under the complex propagation environment. It can be noted for Fig. 2(a)–(d) that the SS-MUSIC method achieves a lower estimation performance compared to the relax method, the algorithm described in [21], and the proposed method for both target heights. This is because the decorrelation preprocess in SS-MUSIC reduces its angular resolution. In addition, the method described in [21] and the relax method show similar performance when the SNR is less than 12 dB, with

This article has been accepted for publication in a future issue of this journal, but has not been fully edited. Content may change prior to final publication. Citation information: DOI 10.1109/TGRS.2021.3131327, IEEE Transactions on Geoscience and Remote Sensing

Accepted Manuscript
Version of record at: https://doi.org/10.1109/TGRS.2021.3131327

TABLE III
EXPERIMENT SETUP FOR THE SECOND SIMULATION

Parameters	Value or mode
Polarization pattern	Horizontal polarization
Height of the array center	80 m
Number of snapshots	64
Interference source direction	$\theta_{\mathrm{im}} - \theta_{\mathrm{3dB}}/2$ and $\theta_{\mathrm{tar}} + \theta_{\mathrm{3dB}}/2$
Included angles of the reflecting paths	0° and 3°
Reflection point height	5 m and 15 m
Relative dielectric constant	4 and 7
Number of iterations	10
Conductivity	1×10^{-5} S/m and 4×10^{-2} S/m
Standard deviation	0.2 m and 0.4 m
Target distance	80 km
Target height	6 km and 9 km
Halt threshold	10^{-5}

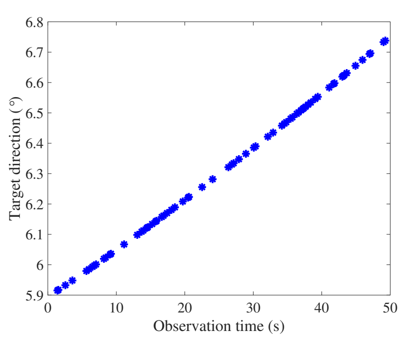

Fig. 4. Target direction relative to the radar site versus the observation time.

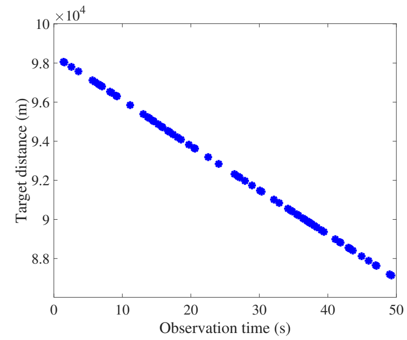

Fig. 5. Target distance relative to the radar site versus the observation time.

the proposed method out-performing other baseline methods. The results in Fig. 2 show that satisfactory classification performance can be achieved by the proposed method under SNR between 0 to 20 dB. It is useful to note that the relax method and that described in [21] may suffer from degradation in localization performance under practical scenarios since they lack path association ability. The proposed method, on the other hand, can achieve satisfactory target classification and localization performance under the mixed interference scenario (such as the scenario considered in this simulation) without using any prior information associated with the multipath propagation environment.

To investigate the effectiveness of the proposed method in a more complex but generalized environment, a complex terrain environment and closely spaced interfering sources are employed in next simulation. Without loss of generality, spatial distribution of the illuminated terrain is unknown a priori. Parameters associated with this simulation setup are listed in Table III, where θ_{3dB}, θ_{tar}, and θ_{im} denote the half-power beamwidth (HPBW), the computed target direction, and the maximal angle of a reflecting path in the environment considered, respectively.

Variations of RMSE with SNR are shown in Fig. 3(a)–(b) for a target located at a distance 80 km from radar with a height of 6 km and in Fig. 3(c)–(d) for a target height of 9 km. We note that neither the SS-MUSIC method nor the relax method can perform effectively under low SNR conditions; they are not capable of achieving an accurate estimate of the target location under this condition. In addition, the baseline methods achieve almost similar performance when SNR is higher than 6 dB. In addition, the variation in performance of the method described in [21] may be attributed to the joint effect of the uneven ground reflections and the closely spaced interferers. We can also note from Fig. 3(a)–(d) that the RML method can hardly estimate the target location for both target height conditions due to the significant model mismatch. These results also highlight that the proposed method outperforms other baseline methods under the same SNR condition. It is also important to note that information pertaining to path association is unknown in practice but is required when implementing the baseline algorithms unlike the proposed method which does not require such information. Therefore, Fig. 3 also indicates that the proposed method can achieve satisfactory classification performance under low SNR conditions. It is

This article has been accepted for publication in a future issue of this journal, but has not been fully edited. Content may change prior to final publication. Citation information: DOI 10.1109/TGRS.2021.3131327, IEEE Transactions on Geoscience and Remote Sensing

Accepted Manuscript
Version of record at: https://doi.org/10.1109/TGRS.2021.3131327

worth emphasizing that any path association information only facilitates the discrimination of target from the detected paths but does not mitigate any detrimental effect contributed by mixed interference. These results indicate that the proposed method can effectively classify and localize the target (under the considered scenario) without the need of prior information associated with the multipath propagation environment. This advantage makes the proposed method attractive, especially for scenarios with mixed interferers. The proposed method can still outperform baseline algorithms in the presence of two sets of multipath signals.

B. Experiment Results via Measured Data

We present results obtained from a real dataset collected by an array radar system with eight channels to validate the effectiveness of the proposed method in a practical environment. It is worth highlighting that the radar system was set up in a geographical environment where ground reflections exist.

After performing several preprocessing tasks such as pulse compression, moving target indication, and constant false alarm detection, the direction and distance of the target relative to the radar site are shown across observation time in Figs. 4 and 5, respectively. We note that the target direction varies from 5.9° to 6.7° and the target distance from 98.1 km to 87.1 km across the observation duration. We also compare the performance of the proposed method to baseline algorithms mentioned in Section V-A with a step-size of 0.01° under various scenarios. It is worth mentioning that the proposed algorithm achieves similar performance when the step-size is varied between 0.002° and 0.01° for the measured data. The results with different step-sizes are not included here due to the space constrain. Estimated target location parameters achieved by different methods are shown in Fig. 6(a) and (b), where the dashed lines denote the real target direction and height, respectively.

It can be noted form Fig. 6 that the RML, the relax, and the SS-MUSIC methods are adversely affected by the complex environment during almost the entire observation time. This implies that the three baseline methods can hardly estimate accurate target location in a real scenario. On the contrary, localization performance of the method described in [21] and the proposed method outperform that of the other three methods. In particular, the proposed method can effectively eliminate the detrimental effect of the convoluted interferences and achieves higher localization accuracy. The time variation of the estimation errors of target location parameters is shown in Fig. 7(a) and (b). These results demonstrate that the proposed method achieves a relatively consistent estimation performance during the entire observation time; it outperforms the baseline methods in terms of estimation accuracy and robustness.

Statistical result of the estimation percentage across different threshold values for different methods is shown in Fig. 8. It can be observed that the estimation percentage achieved by the proposed method is significantly higher than that achieved by the other four methods. The proposed method can achieve a 98% rate when the comparison threshold is larger than 240 m. In contrast, when the comparison threshold is equal

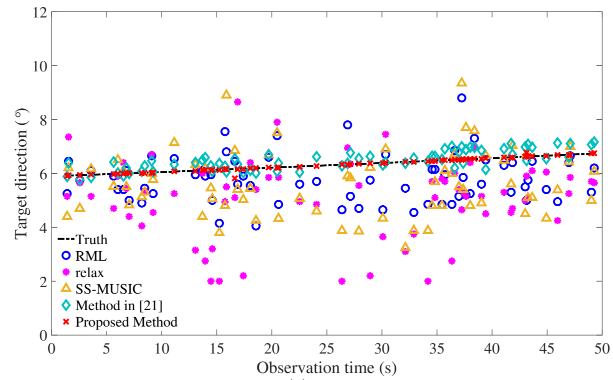

(a)

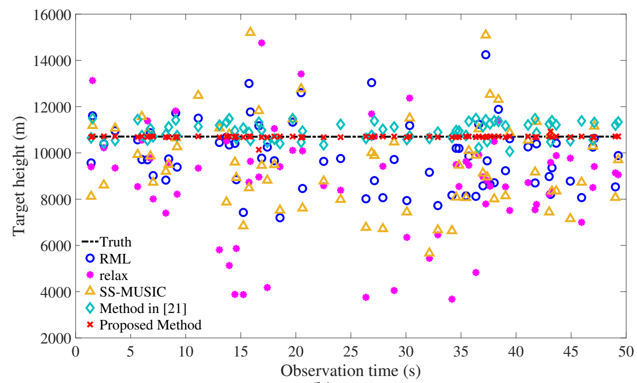

(b)

Fig. 6. Location parameter estimation results versus the observation time via measured data. (a) Estimation result of target angle produced by different methods. (b) Estimation result of target height produced by different methods.

to 240 m, the estimation percentages achieved by the RML, the relax, the SS-MUSIC methods, and that described in [21] are 7.3%, 5.8%, 10.1%, and 37.7%, respectively. These results based on measured data demonstrate that the proposed method can achieve target localization under a practical environment without any prior knowledge of the propagation environment.

VI. Conclusions

We investigated the target localization problem under a complex interference environment. Motivated by the lack of prior information in practical applications, we first formulate a generalized propagation relationship based on the spherical Earth model, where the non-ideal assumption of the classical two-ray multipath propagation model can be avoided, and the robustness of the propagation model in the practical environment is enhanced. A new target localization method based on the iterative implementation of the MMSE framework with semi-unitary constraint and eigen-decomposition technique is proposed to mitigate the influence of mixed interference on the target localization accuracy. The main advantage of the proposed method is that it can automatically distinguish the target from the mixed interference environment and significantly improve the accuracy of the target location estimates without requiring additional decorrelation preprocessing nor prior information pertaining to the dynamic propagation environment. Simulation and experiment results based on both

This article has been accepted for publication in a future issue of this journal, but has not been fully edited. Content may change prior to final publication. Citation information: DOI 10.1109/TGRS.2021.3131327, IEEE Transactions on Geoscience and Remote Sensing

Accepted Manuscript
Version of record at: https://doi.org/10.1109/TGRS.2021.3131327

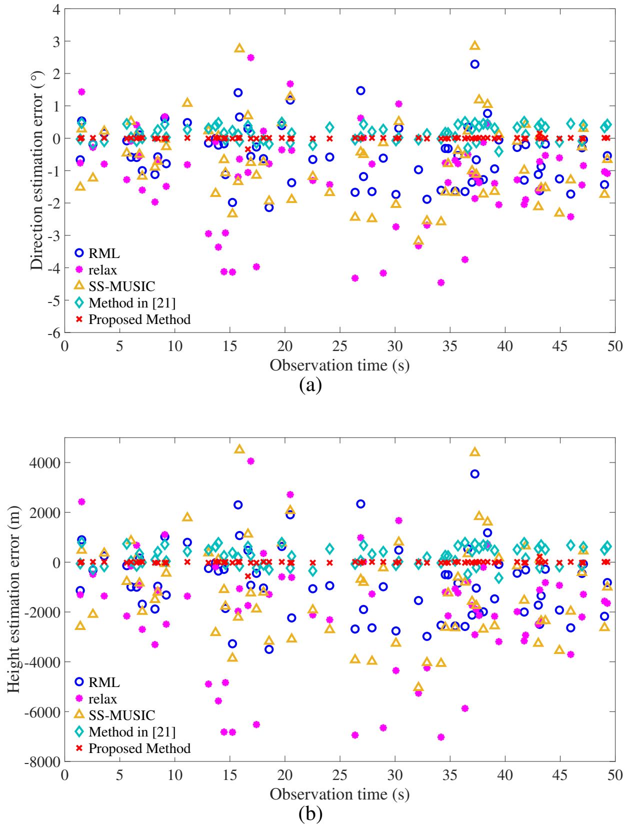

Fig. 7. Estimation errors of location parameters versus the observation time via measured data. (a) Estimation error of target angle produced by different methods. (b) Estimation error of target height produced by different methods.

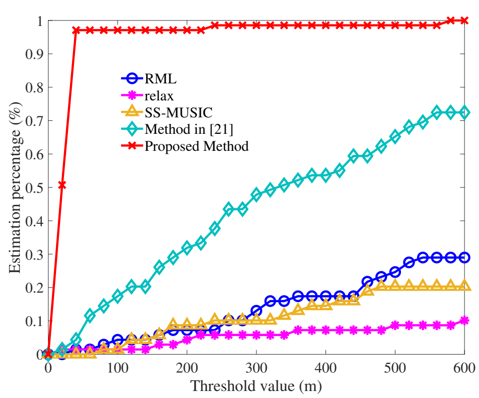

Fig. 8. Relationships between the estimation percentage and different threshold values for different methods.

synthetic and measured data showed improved performance in terms of localization accuracy for the proposed method.

Appendix A

Define $\boldsymbol{\theta}_1 = [\theta_{\rm tar}, \theta_{{\rm in},1}, \cdots, \theta_{{\rm in},i}, \cdots, \theta_{{\rm in},I}]^T$ consisting DOAs of the target and the interference sources, and $\boldsymbol{\theta}_2 = [\theta_{{\rm im},1}, \cdots, \theta_{{\rm im},k}, \cdots, \theta_{{\rm im},K}]^T$ consisting DOAs of the reflecting paths. Matrix $\mathbf{B}$ can be rewritten by

$$\mathbf{B} = [\mathbf{A}_{\boldsymbol{\theta}_{\rm tar}}\boldsymbol{\rho}, \mathbf{A}_{\boldsymbol{\theta}_{\rm int}}] = [\mathbf{A}_{\boldsymbol{\theta}_1}, \mathbf{A}_{\boldsymbol{\theta}_2}] \begin{bmatrix} \mathbf{I}_{I+1} \\ \mathbf{M} \end{bmatrix}, \tag{52}$$

where $\mathbf{I}_{I+1}$ is the $(I+1)\times(I+1)$ identity matrix and $\mathbf{M} = \left[\boldsymbol{\rho}_{\backslash\bar{\rho}_0}, \mathbf{O}_{K\times I}\right] \in \mathbb{C}^{K\times(I+1)}$ with $\mathbf{O}_{K\times I}$ denoting the all-zero matrix of size $K+I$. Since the matrix $[\mathbf{A}_{\boldsymbol{\theta}_1}, \mathbf{A}_{\boldsymbol{\theta}_2}]$ is of full column rank if $M \geq I+K+1$, with reference to (52), matrix $\mathbf{B}$ is of full column rank and rank $\left(\mathbf{B}\mathbf{R}_s\mathbf{B}^H\right) = {\rm rank}\left(\mathbf{B}\right) = I+1$ since $\mathbf{R}_s$ is positive-definite. The proof is completed.

Appendix B

Assume $\mathbf{a}\left(\theta_{\rm tar}\right) \in {\rm span}\left(\mathbf{U}_s\right)$. According to (40), there must exist a nonzero vector $\mathbf{h} = [h_1, h_2, \cdots, h_{I+1}]^T$ that yields

$$\mathbf{B}\mathbf{h} = [\mathbf{A}_{\boldsymbol{\theta}_{\rm tar}}\boldsymbol{\rho}, \mathbf{A}_{\boldsymbol{\theta}_{\rm int}}]\,\mathbf{h} = \mathbf{a}\left(\theta_{\rm tar}\right). \tag{53}$$

Let $\mathbf{h}_{\backslash h_1} = [h_2, \cdots, h_{I+1}]^T$ with $\backslash h_1$ denoting the removal of h_1 from $\mathbf{h}$, (53) can then be rewritten by

$$\begin{aligned}[\mathbf{A}_{\boldsymbol{\theta}_{\rm tar}}\boldsymbol{\rho}, \mathbf{A}_{\boldsymbol{\theta}_{\rm int}}]\,\mathbf{h} - \mathbf{a}\left(\theta_{\rm tar}\right) &= [\mathbf{A}_{\boldsymbol{\theta}_{\rm tar}}, \mathbf{A}_{\boldsymbol{\theta}_{\rm int}}] \\ &\times \begin{bmatrix} h_1\boldsymbol{\rho} - \tilde{\boldsymbol{\rho}}_{\rm tar} \\ \mathbf{h}_{\backslash h_1} \end{bmatrix} = \mathbf{0},\end{aligned} \tag{54}$$

where $\tilde{\boldsymbol{\rho}}_{\rm tar} = [1, 0, \cdots, 0]^T$ of size $(K+1)\times 1$. Since the matrix $[\mathbf{A}_{\boldsymbol{\theta}_{\rm tar}}, \mathbf{A}_{\boldsymbol{\theta}_{\rm int}}]$ is of full column rank if $M \geq I+K+1$, (54) implies that $\boldsymbol{\rho}_{\backslash\bar{\rho}_0} = [\bar{\rho}_1, \cdots, \bar{\rho}_k, \cdots, \bar{\rho}_K]^T = \mathbf{0}$ and $\mathbf{h}_{\backslash h_1} = \mathbf{0}$, which contradicts the assumption of $\boldsymbol{\rho}_{\backslash\bar{\rho}_0} \neq \mathbf{0}$. Thus, we have $\mathbf{a}\left(\theta_{\rm tar}\right) \notin {\rm span}\left(\mathbf{U}_s\right)$.

Similarly, assume $\mathbf{a}\left(\theta_{{\rm im},k}\right) \in {\rm span}\left(\mathbf{U}_s\right)$. According to (40), there exist a nonzero vector $\mathbf{r} = [r_1, r_2, \cdots, r_{I+1}]^T$ that yields

$$\mathbf{B}\mathbf{r} = [\mathbf{A}_{\boldsymbol{\theta}_{\rm tar}}\boldsymbol{\rho}, \mathbf{A}_{\boldsymbol{\theta}_{\rm int}}]\,\mathbf{r} = \mathbf{a}\left(\theta_{{\rm im},k}\right),\ k = 1, 2, \cdots, K. \tag{55}$$

Let $\mathbf{r}_{\backslash r_1} = [r_2, \cdots, r_{I+1}]^T$ with $\backslash r_1$ denoting the removal of r_1 from $\mathbf{r}$, (55) can then be rewritten as

$$\begin{aligned}[\mathbf{A}_{\boldsymbol{\theta}_{\rm tar}}\boldsymbol{\rho}, \mathbf{A}_{\boldsymbol{\theta}_{\rm int}}]\,\mathbf{r} - \mathbf{a}\left(\theta_{{\rm im},k}\right) &= [\mathbf{A}_{\boldsymbol{\theta}_{\rm tar}}, \mathbf{A}_{\boldsymbol{\theta}_{\rm int}}] \\ &\times \begin{bmatrix} r_1\boldsymbol{\rho} - \tilde{\boldsymbol{\rho}}_{\rm im} \\ \mathbf{r}_{\backslash r_1} \end{bmatrix} = \mathbf{0},\end{aligned} \tag{56}$$

where $\tilde{\boldsymbol{\rho}}_{\rm im} = [0, \cdots, 0, 1, 0, \cdots, 0]^T$ is a zero vector of size $(K+1)\times 1$ with a single value of one positioned at the $(k+1)$th element. Since matrix $[\mathbf{A}_{\boldsymbol{\theta}_{\rm tar}}, \mathbf{A}_{\boldsymbol{\theta}_{\rm int}}]$ is of full column rank if $M \geq I+K+1$, (56) implies that $r_1 = 0$ and $\mathbf{r}_{\backslash r_1} = \mathbf{0}$, which contradicts the assumption of $\mathbf{r} \neq \mathbf{0}$. Thus, we have $\mathbf{a}\left(\theta_{{\rm im},k}\right) \notin {\rm span}\left(\mathbf{U}_s\right)$ and the proof is completed.

References

[1] J. Zhao, Y. Tian, B. Wen, and Z. Tian, "Coherent DOA estimation in sea surface observation with direction-finding HF radar," *IEEE Trans. Geosci. Remote Sens.*, (Early Access), doi: 10.1109/TGRS.2020.3028074.

[2] U. Nielsen, J. Yan, S. Gogineni, and J. Dall, "Direction-of-arrival analysis of airborne ice depth sounder data," *IEEE Trans. Geosci. Remote Sens.*, vol. 55, no. 4, pp. 2239–2249, Apr. 2017.

[3] A. Sahin and E. L. Miller, "Object detection using high resolution near-field array processing," *IEEE Trans. Geosci. Remote Sens.*, vol. 39, no. 1, pp. 136–141, Jan. 2001.

[4] J. C. West and Z. Zhao, "Electromagnetic modeling of multipath scattering from breaking water waves with rough faces," *IEEE Trans. Geosci. Remote Sens.*, vol. 40, no. 3, pp. 583–592, Mar. 2002.

[5] J. C. West, "Ray analysis of low-grazing scattering from a breaking water wave," *IEEE Trans. Geosci. Remote Sens.*, vol. 37, no. 6, pp. 2725–2727, Nov. 1999.

[6] D. Rahamim, J. Tabrikian, and R. Shavit, "Source localization using vector sensor array in a multipath environment," *IEEE Trans. Signal Process.*, vol. 52, no. 11, pp. 3096–3103, Nov. 2004.

[7] H. Naseri and V. Koivunen, "Cooperative simultaneous localization and mapping by exploiting multipath propagation," *IEEE Trans. Signal Process.*, vol. 65, no. 1, pp. 200–211, Jan. 2017.

[8] F. Liu, J. Wang, C. Sun, and R. Du, "Spatial differencing method for DOA estimation under the coexistence of both uncorrelated and coherent signals," *IEEE Trans. Antennas Propag.*, vol. 60, no. 4, pp. 2052–2062, Apr. 2012.

[9] S. Valaee and P. Kabal, "The optimal focusing subspace for coherent signal subspace processing," *IEEE Trans. Signal Process.*, vol. 44, no. 3, pp. 752–756, Mar. 1996.

[10] H. Park, V. González-Gambau, A. Camps, and M. Vall-llossera, "Improved MUSIC-based SMOS RFI source detection and geolocation algorithm," *IEEE Trans. Geosci. Remote Sens.*, vol. 54, no. 3, pp. 1311–1322, Mar. 2016.

[11] R. O. Schmidt, "A signal subspace approach to multiple emitter location and spectral estimation," Ph.D. dissertation, Stanford Univ., Stanford, CA, USA, 1981.

[12] S. U. Pillai and B. H. Kwon, "Forward/backward spatial smoothing techniques for coherent signal identification," *IEEE Trans. Acoust., Speech, Signal Process.*, vol. 37, no. 1, pp. 8–15, Jan. 1989.

[13] Z. Zhou, M. G. Christensen, J. R. Jensen, and H. C. So, "Joint DOA and fundamental frequency estimation based on relaxed iterative adaptive approach and optimal filtering," in *Proc. IEEE Int. Conf. Acoust., Speech, Signal Process. (ICASSP)*, Vancouver, BC, Canada, May 2013, pp. 6812–6816.

[14] A. Hizal and S. Koc, "Mitigating the multipath effects of low angle monopulse tracking by even difference pattern," in *Proc. Eur. Radar Conf.*, Amsterdam, Netherlands, Oct. 2012, pp. 290–293.

[15] T. Lo and J. Litva, "Use of a highly deterministic multipath signal model in low-angle tracking," *IEE Proc. F-Radar Signal Process.*, vol.138, no. 2, pp. 163–171, Apr. 1991.

[16] A. Aubry, V. Carotenuto, A. De Maio, and L. Pallotta, "Localization in 2D PBR with multiple transmitters of opportunity: a constrained least squares approach," *IEEE Trans. Signal Process.*, vol. 68, pp. 634–646, Jan. 2020.

[17] A. Aubry, P. Braca, A. Demaio, and A. Marino, "2D PBR localization complying with constraints forced by active radar measurements," *IEEE Trans. Aerosp. Electron. Syst.*, vol. 57, no. 5, pp. 2647–2660, Oct. 2021.

[18] A. Aubry, P. Braca, A. D. Maio, and, A. Marino, "Enhanced target localization with deployable multiplatform radar nodes based on non-convex constrained least squares optimization," [Online]. Available: https://arxiv.org/abs/2104.11209

[19] Y. Liu, B. Jiu, X.-G. Xia, H. Liu, and L. Zhang, "Height measurement of low-angle target using MIMO radar under multipath interference," *IEEE Trans. Aerosp. Electron. Syst.*, vol. 54, no. 2, pp. 808–818, Apr. 2018.

[20] Y. Liu, H. Liu, X.-G. Xia, L. Zhang, and B. Jiu, "Projection techniques for altitude estimation over complex multipath condition based VHF radar," *IEEE J. Sel. Topics Appl. Earth Obs. Remote Sens.*, vol. 11, no. 7, pp. 2362–2375, Jul. 2018.

[21] Y. Liu, H. Liu, L. Wang, and G. Bi, "Target localization in high-coherence multipath environment based on low-rank decomposition and sparse representation," *IEEE Trans. Geosci. Remote Sens.*, vol. 58, no. 9, pp. 6197–6209, Sept. 2020.

[22] D. B. Trizna, "A model for brewster angle damping and multipath effects on the microwave radar sea echo at low grazing angles," *IEEE Trans. Geosci. Remote Sens.*, vol. 35, no. 5, pp. 1232–1244, Sep. 1997.

[23] M. L. Meeks, *Radar Propagation at Low Altitude*, Dedham, MA, USA: Artech House, 1982.

[24] J. G. Teti, "Wide-band airborne radar operating considerations for low-altitude surveillance in the presence of specular multipath," *IEEE Trans. Antennas Propag.*, vol. 48 no. 2, pp. 176–191, Feb. 2000.

[25] G. A. Watson and D. H. Mccabe, "Benchmark problem with a multisensory framework for radar resource allocation and tracking of highly maneuvering targets, closely-spaced targets, and targets in the presence of sea-surface-induced multipath," Defense Tech. Inf. Center, Fort Belvoir, VA, USA, Tech. Rep. NSWCDD/TR-99/32, May 1999.

[26] D. Zhu, X. Peng, and G. Li, "A matrix completion based method for RFI source localization in microwave interferometric radiometry," *IEEE Trans. Geosci. Remote Sens.*, (Early Access), doi: 10.1109/TGRS.2020.3033842.

[27] J. Li, F. Hu, F. He, and L. Wu, "High-resolution RFI localization using covariance matrix augmentation in synthetic aperture interferometric radiometry," *IEEE Trans. Geosci. Remote Sens.*, vol. 56, no. 2, pp. 1186-1198, Feb. 2018.

[28] D. Zhu, J. Li, and G. Li, "RFI source localization in microwave interferometric radiometry: a sparse signal reconstruction perspective," *IEEE Trans. Geosci. Remote Sens.*, vol. 58, no. 6, pp. 4006-4017, June 2020.

[29] W. D. Blair and M. Brandt-pearce, "Statistic of monopulse measurements of Rayleigh targets in the presence of specular and diffuse multipath," in *Proc. IEEE Radar Conf.*, Atlanta, GA, USA, May 2001, pp. 369–375.

[30] W. Jiang, M. Zhang, P. Wei, and D. Nie, "Spectral decomposition modeling method and its application to EM scattering calculation of large rough surface with SSA method," *IEEE J. Sel. Topics Appl. Earth Observ. Remote Sens.*, vol. 8, no. 4, pp. 1848–1854, Apr. 2015.

[31] R. Takahashi, K. Hirata, and H. Maniwa, "Altitude estimation of low elevation target over the sea for surface based phased array radar," in *Proc. IEEE Radar Conf.*, Arlington, VA, USA, May 2010, pp. 123–128.

[32] C. Bourlier and G. Kubické, "Ground wave propagation along an inhomogeneous rough surface in the HF band: Millington effect for a flat earth," *IEEE Trans. Geosci. Remote Sens.*, vol. 49, no. 4, pp. 1374–1382, Apr. 2011.

[33] D. Y. Northam, "A stochastic simulation of low grazing angle, forward scatter, over-water multipath effects," Naval Res. Lab., Washington, DC, USA, Tech. Rep. 5658, Dec. 1981.

[34] R. Gribonval and M. Nielsen, "Sparse representation in unions of bases," *IEEE Trans. Inf. Theory.*, vol. 49, no. 12, pp. 3320–3325, Dec. 2003.

[35] R. Heylen, A. Zare, P. Gader, and P. Scheunders, "Hyperspectral unmixing with endmember variability via alternating angle minimization," *IEEE Trans. Geosci. Remote Sens.*, vol. 54, no. 8, pp. 4983–4993, Aug. 2016.

[36] M. V. Afonso, J. M. Bioucas-Dias, and M. A. T. Figueiredo, "An augmented Lagrangian approach to the constrained optimization formulation of imaging inverse problems," *IEEE Trans. Image Process.*, vol. 20, no. 3, pp. 681–695, Mar. 2011.

[37] Q. Zhao, Q. Du, W. Sun, and Y. Chen, "Iterative double laplacian-scaled low-rank optimization for under-sampled and noisy signal recovery," *IEEE Trans. Geosci. Remote Sens.*, vol. 57, no. 11, pp. 9177–9187, Nov. 2019.

[38] H. Krim and M. Viberg, "Two decades of array signal processing research: the parametric approach," *IEEE Signal Process. Mag.*, vol. 13, no. 4, pp. 67–94, Jul. 1996.

[39] A. H. T. Nguyen, V. G. Reju, and A. W. H. Khong, "Directional sparse filtering for blind estimation of under-determined complex-valued mixing matrices," *IEEE Trans. Signal Process.*, vol. 68, pp. 1990–2003, Mar. 2020.

[40] Y. E. Nesterov, "A method for solving the convex programming problem with convergence rate O (1/kˆ2)," Dokl. akad. Nauk Sssr, vol. 269, pp. 543–547, 1983.

[41] H. Yan and H. H. Fan, "On source association of DOA estimation under multipath propagation," *IEEE Signal Process. Lett.*, vol. 12, no. 10, pp. 717–720, Oct. 2005.

[42] M. Wax and T. Kailath, "Detection of signals by information theoretic criteria," *IEEE Trans. Acoust., Speech, Signal Process.*, vol. 33, no. 2, pp. 387–392, Apr. 1985.

[43] Y. Long, J. Lin, B. Li, H. Wang, and Z. Chen, "Fast-AIC method for automatic first arrivals picking of microseismic event with multitrace energy stacking envelope summation," *IEEE Trans. Geosci. Remote Sens. Lett.*, vol. 17, no. 10, pp. 1832–1836, Oct. 2020.

[44] A. Mariani, A. Giorgetti, and M. Chiani, "Model order selection based on information theoretic criteria: design of the penalty," *IEEE Trans. Signal Process.*, vol. 63, no. 11, pp. 2779–2789, Jun. 2015.

[45] L. Yu, W. Liu, and R. Langley, "A novel robust beamformer based on sub-array data subtraction for coherent interference suppression," in *Proc. IEEE/SP 15th Workshop on Statistical Signal Processing*, Cardiff, UK, Sept. 2009, pp. 525–528.

[46] Yang-Ho Choi,"Improved adaptive nulling of coherent interference without spatial smoothing," *IEEE Trans. Signal Process.*, vol. 52, no. 12, pp. 3464–3469, Dec. 2004.

[47] Q. J. O. Tan and R. A. Romero, "Airborne target detection using dual matched filter discriminator with matched waveform illumination for

coherent jammer suppression," in *Proc. IEEE Radar Conf.*, Boston, MA, USA, Apr. 2019, pp. 1–6.